

Dirac Spectra and Edge States in Honeycomb Plasmonic Lattices

Dezhuan Han,¹ Yun Lai,¹ Jian Zi,² Zhao-Qing Zhang,¹ and C. T. Chan¹

¹*Department of Physics, Hong Kong University of Science and Technology, Clear Water Bay, Kowloon, Hong Kong, China*

²*Department of Physics, Fudan University, Shanghai 200433, People's Republic of China*

(Received 30 July 2008; revised manuscript received 25 January 2009; published 26 March 2009)

We study theoretically the dispersion of plasmonic honeycomb lattices and find Dirac spectra for both dipole and quadrupole modes. Zigzag edge states derived from Dirac points are found in ribbons of these honeycomb plasmonic lattices. The zigzag edge states for out-of-plane dipole modes are closely analogous to the electronic ones in graphene nanoribbons. The edge states for in-plane dipole modes and quadrupole modes, however, have rather unique characters due to the vector nature of the plasmonic excitations. The conditions for the existence of plasmonic edge states are derived analytically.

DOI: 10.1103/PhysRevLett.102.123904

PACS numbers: 42.70.Qs, 41.20.Jb, 73.20.Mf

Metal nanoparticles support remarkable optical resonances known as localized surface plasmons [1,2]. Surface plasmons are collective electronic density waves bound at metal surfaces that can locally enhance incident optical fields by orders of magnitude. The enhanced optical fields in the near field give rise to many extraordinary optical phenomena such as surface-enhanced Raman scattering [3,4] and single-molecule fluorescence detection [5]. The arrangement of metal nanoparticles regularly can offer more. It has been shown that a chain of closely spaced metal nanoparticles can guide electromagnetic (EM) energy with lateral mode confinement below the diffraction limit [6]. Two-dimensional lattices consisting of metal nanoparticles show interesting tunable optical response over the entire visible range [7]. A three-dimensional arrangement of metal nanoparticles can form metallic photonic crystals (PCs) with robust photonic band gaps that depend on the local order rather than on the symmetry or the global long range order [8]. Metal nanoparticles thus manifest promising building blocks for plasmonic materials, leading to unprecedented applications in nanophotonics, nonlinear optics, biosensing, and even medical therapy.

Recently, graphene has received considerable interest because of the existence of the Dirac point that offers remarkable electronic properties [9–11]. The Dirac spectra in 2D PCs for EM waves have also been identified [12,13] and the Dirac-point-derived edge states have novel transportation properties when time-reversal symmetry breaking is introduced. These edge states can render “one-way” waveguiding for EM waves, confirmed by numerical simulations [14]. Both graphene and 2D PCs support Dirac dispersions. However, the Dirac spectrum in graphene is derived directly from the nearest-neighbor hopping of bound electron states, while that in 2D PCs corresponds to the photonic bands of scattering photons.

In this Letter, we study theoretically the plasmonic band structures of metal nanospheres arranged in a honeycomb lattice. The plasmonic lattice is an open system that supports both guided modes and leaky modes [15], and as

such, it is different from electronic graphene and 2D PCs. Furthermore, the Dirac dispersions found in graphene and 2D PCs are only for scalar waves. The 2D plasmonic lattice can support both scalar waves and vector waves. Our results reveal that for both scalar and vector waves, this honeycomb plasmonic lattice possesses Dirac points for the infinite system and guided edge states when an edge is present. The edge states provide additional transport channels other than the bulk states, which can even lead to one-way waveguide. Other properties such as antilocalization and size-dependent density of states should also be interesting. Some behaviors of the plasmonic edge states can be very different from that in graphene electronics. The existence of Dirac points and edge states in plasmonic systems may open up new avenues in both physics and applications for the emerging field of plasmonics.

The honeycomb plasmonic structure under study is shown in Fig. 1(a), in which each black dot in the x - y plane represents a metal sphere. Its Brillouin zone (BZ) is shown in Fig. 1(b). The interdistance between adjacent spheres is $a_0 = a/\sqrt{3}$, where a is the lattice constant. We use the Drude-type permittivity $\varepsilon(\omega) = 1 - \omega_p^2/\omega^2$ with $\omega_p = 6.18$ eV for metal spheres. The lattice constant is chosen to be $a = 60$ nm, and the sphere radius is $r_s = 10$ nm. At this ratio of $r_s/a = \sqrt{3}/6$, the bands derived from dipole and quadrupole resonances are separated in energy as demonstrated below. As the coupling between different angular momentum channels is weak, the bands can be meaningfully assigned as dipole and quadrupole bands.

The plasmonic dipole dispersions calculated within the quasistatic approximation (QSA) limit are shown in Fig. 1(c), in which the gray (red) lines are for out-of-plane \mathbf{P}_{out} modes and the black lines correspond to in-plane \mathbf{P}_{in} modes. The \mathbf{P}_{in} and \mathbf{P}_{out} modes form their own orthogonal subspaces. We see that there are two Dirac cones at the K point, one for the \mathbf{P}_{in} and one for the \mathbf{P}_{out} modes. Figure 1(d) shows the plasmonic dispersions in the QSA limit if only quadrupoles (\mathbf{Q}) are considered, where a Dirac

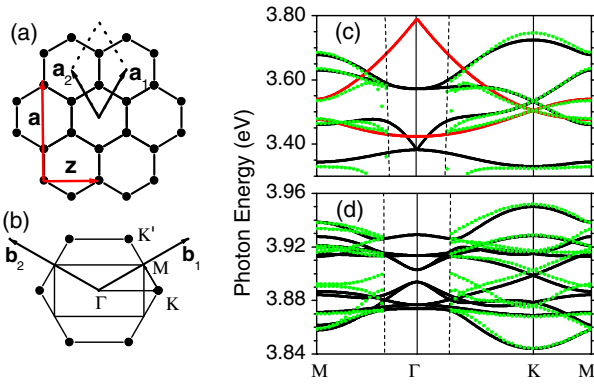


FIG. 1 (color online). (a) Schematic structure of the honeycomb plasmonic lattice. \mathbf{a}_1 , \mathbf{a}_2 are the primitive vectors; \mathbf{z} is the 1D primitive vector for zigzag ribbons. (b) Reciprocal lattice vectors. (c) QSA band structures for in-plane dipole modes (black lines) and out-of-plane dipole modes (red lines). (d) QSA band structures for quadrupoles. MST results (electrodynamic calculation with retardation effects taken fully into account) are also shown in (c) and (d) by green dots. The dashed lines in (c) and (d) indicate the light lines. The lattice constant is 60 nm and the sphere radius is 10 nm.

point can also be found. At these Dirac points, the constant frequency surfaces are represented by two cones meeting at the K point. It should be pointed out that the in-plane dipole and quadrupole modes are vector waves in nature. The existence of Dirac dispersions in these cases is a result of the symmetry of the honeycomb structure which is robust against their vector nature.

We note that the l th multipole plasmon resonance frequency of a small plasmonic sphere is $\omega_l = [l/(2l+1)]^{1/2} \omega_p$. When the spheres are arranged in a lattice, each multipole resonance couples to form a set of bands, and these manifolds do not mix when r_s/a_0 is small. The dipole and quadrupole bands shown in Fig. 1 are indeed separated in energy. In Figs. 1(c) and 1(d), we compare the QSA results with the fully fledged multiple scattering theory (MST) results (shown by green dots) [16] for dipole and quadrupole modes, respectively. The MST gives a solution to Maxwell's equations that takes into account the full retardation effects. The MST dispersions are shown only for $k > \omega/c$, since that for the leaky modes inside the light cone are not well defined due to the coupling with free photons. As the K point is far away from light cone, the Dirac dispersions found by QSA agree well with the MST calculations. We will discuss the Dirac dispersions with QSA since it can give a more straightforward interpretation.

An important consequence of the Dirac spectrum in graphene electronics is the existence of peculiar edge states [11] with unusual physical properties [10] in graphene ribbons with finite widths. Two types of graphene nano-ribbons, namely, zigzag and armchair ribbons, are usually considered. In Fig. 1(a), the vector \mathbf{z} (a) indicates the

translation vector of the zigzag (armchair) ribbons, and the longer (shorter) side of the rectangle inside the 2D graphene BZ is the 1D BZ of the zigzag (armchair) ribbons. The band structure of the zigzag (armchair) graphene ribbons can be predicted by the projection of 2D graphene bands onto the corresponding axis of the reciprocal lattice vector. The original Dirac point K (K') is expected to appear at $ka = 2\pi/3$ (0) for zigzag (armchair) ribbons. Compared with the projected 2D electronic graphene bands, a new feature of zigzag ribbons is the appearance of edge states that extends from $ka = \pi$ to $2\pi/3$, where $ka = 2\pi/3$ is the expected degeneracy point of the 2D projected graphene bands. These new additional edge states form a flat band at energy $E = 0$ with wave functions localized near the edge sites. Within a tight-binding model, the necessary condition for $E = 0$ edge states is “zero hopping”; namely, the total sum of hopping terms over the nearest-neighbor sites should vanish. In this way the condition $ka > 2\pi/3$ for the existence of zigzag edge states can be proved analytically.

We now discuss the Dirac-point-derived edge states of plasmonic ribbons. The results for finite-width plasmonic ribbons here are calculated for $N = 10$ zigzag ribbons, where N is an integer characterizing the width of the ribbon [11]. We expect that the edge states of out-of-plane modes might be similar to those of electronic edge states derived from the out-of-plane π states in graphene, while the edge states for the \mathbf{P}_{in} and \mathbf{Q} modes (if there are any) might be very different. We note that electronic graphene [11] and 2D PCs studied recently [13] are all dealing with scalar waves. In their cases, the electron and photon transport near the Dirac points can be described by the “two-component” massless Dirac Hamiltonian $\mathbf{H} = \hbar v_F (k_x \sigma_x + k_y \sigma_y)$, where v_F is a band parameter and σ is the Pauli matrix. In the plasmonic sphere arrays, the vector nature of EM waves enters explicitly, and the underlying physics may go beyond the “two-component” Dirac equation.

In Fig. 2, the blue lines represent the plasmonic bands of zigzag ribbons for out-of-plane dipole, in-plane dipole, and quadrupole. The bands are superimposed on top of the plasmonic bands of the 2D honeycomb lattice projected along the zigzag axis, which are shown as the gray background. For \mathbf{P}_{out} modes in Fig. 2(a), we see that the ribbon bands basically overlap the projected 2D bands with the exception of an additional degenerate flat band starting from about $ka = 2\pi/3$ to π in the gap of the projected bands, which corresponds to the edge states in the zigzag graphene ribbons. This flat band occurs at 3.51 eV (the single sphere dipole resonance $\omega_{l=1} = 3.52$ eV), which has the similar physical meaning of $E = 0$ (zero hopping) in graphene. The slight differences in the edge state frequencies and $\omega_{l=1}$ come from the hopping among farther sites in the lattice, which is neglected in the tight-binding model for graphene.

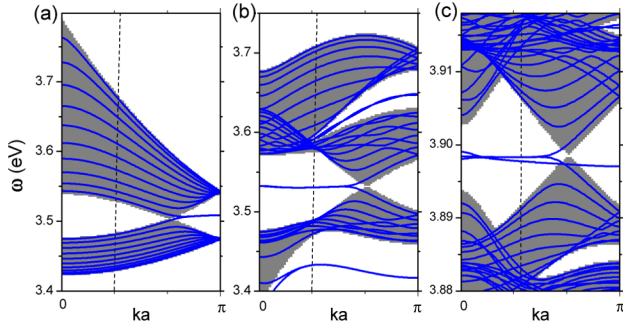


FIG. 2 (color online). Band structures for $N = 10$ zigzag plasmonic ribbons (blue lines) and projected bands for the 2D honeycomb structure along the corresponding reciprocal axis (gray area). (a) Out-of-plane dipole modes. The flat band between $2\pi/3$ and π corresponds to edge states. (b) In-plane dipole modes. The flat band with ka ranging from 0 to $2\pi/3$ corresponds to Dirac-point-derived edge states. (c) Quadrupole modes. There are two bands for edge states: one with ka ranging from 0 to $2\pi/3$, the other traversing the whole BZ. The system parameters are the same as in Fig. 1.

For \mathbf{P}_{in} modes, there is no edge state from $ka = 2\pi/3$ to π ; however, a new additional flat band with its frequency near $\omega_{l=1}$ emerges from $ka = 0$ to about $2\pi/3$. This phenomenon is rather different from that in the zigzag graphene ribbon, where the edge states are forbidden near the Γ point. The two-component effective Dirac equation commonly used in graphene electronics is not valid in this case since the vector nature of EM waves introduces extra degrees of freedom. A more interesting observation can be made when we come to quadrupoles. Two sets of edge states appear near the single particle resonance at $\omega_{l=2} = 3.9$ eV. The dispersion of one set of edge states is similar to the in-plane dipole edge mode discussed above, as it is almost flat and is confined between $0 \leq ka < 2\pi/3$. There is an additional band of edge states with a small and negative group velocity that goes all the way from $ka = 0$ to π .

In the following, we give an analytic derivation of the condition for the existence of plasmonic zigzag edge states near multipole resonance frequencies by truncating the Green function to the nearest neighbor. Let us consider a general tensor field \mathbf{F} of rank l (which can be the electric field in the case of a dipole or the field gradient in the case of a quadrupole) generated by a localized source \mathbf{V} with rank l (dipole, quadrupole, etc.). In free space, the field and the source are related by the $2l$ th rank Green function $\mathbf{G}(\mathbf{r} - \mathbf{r}')$, which satisfies $\mathbf{F}(\mathbf{r}) = \mathbf{G}(\mathbf{r} - \mathbf{r}')\mathbf{V}(\mathbf{r}')$ and the linear response gives $\mathbf{V}(\mathbf{r}) = \alpha\mathbf{F}(\mathbf{r})$, where α is the multipole polarizability. We place these point sources \mathbf{V} on a semi-infinite honeycomb lattice with a zigzag edge as shown in the inset of Fig. 3. The indices (m, n) in the inset are used to label the honeycomb sites, where n and m label the position along (y axis) and perpendicular to (x axis) the zigzag chain, respectively. $\mathbf{r}_{m,n}$ is the coordinate of the

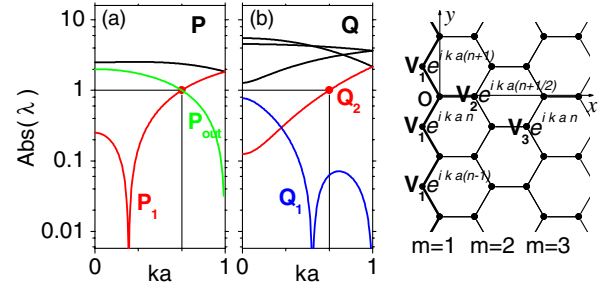


FIG. 3 (color online). Absolute values of eigenvalues λ of the matrix \mathbf{T} as a function of the Bloch wave vector k . \mathbf{V} is either \mathbf{P} or \mathbf{Q} . $|\lambda| < 1$ gives the condition for edge states. (a) Dipole modes. The light gray (green) line is for out-of-plane modes and the dark gray (red) line and the black line are for in-plane modes. (b) Quadrupole modes. \mathbf{Q}_1 (blue curve) is always an edge state, while \mathbf{P}_1 and \mathbf{Q}_2 give edge state solutions when $ka < 2\pi/3$. The inset is a sketch of a semi-infinite honeycomb structure with a zigzag edge. The indices (m, n) and vector wave functions are defined as shown.

(m, n) site, and the site $(1, n + 1/2)$, located between $(1, n)$ and $(1, n + 1)$, is chosen to be the origin. We search for eigenstates with a Bloch wave vector k along the zigzag edge and we demand that the frequency should be equal to the single particle multipole resonance frequency. If we truncate the Green function to the nearest neighbor, the condition for the frequency to be equal to the single particle multipole resonance frequency is zero hopping, namely, a zero sum of the fields from the three nearest neighbors. This gives

$$\mathbf{G}(-\mathbf{r}_{1,n})\mathbf{V}_{1,n} + \mathbf{G}(-\mathbf{r}_{1,n+1})\mathbf{V}_{1,n+1} + \mathbf{G}(-\mathbf{r}_{2,n+1/2})\mathbf{V}_{2,n+1/2} = 0, \quad (1)$$

where $\mathbf{V}_{m,n} = \mathbf{V}_m e^{inka}$ if the periodic Bloch condition is imposed. From Eq. (1) a matrix \mathbf{T} relating \mathbf{V}_1 and \mathbf{V}_2 can be defined as $\mathbf{T} = -\mathbf{G}^{-1}(-\mathbf{r}_{2,n+1/2})[\mathbf{G}(-\mathbf{r}_{1,n})e^{-ika/2} + \mathbf{G}(-\mathbf{r}_{1,n+1})e^{ika/2}]$. This procedure can be done iteratively to obtain $\mathbf{V}_m = \mathbf{T}^{m-1}\mathbf{V}_1$. The eigenvalues of the matrix \mathbf{T} give the properties of the states. If $|\lambda| < 1$, the states are localized edge states, while $|\lambda| = 1$ corresponds to a Bloch state extending to the interior of the ribbon.

For out-of-plane modes, the Green function $\mathbf{G}^{\text{P}}(\mathbf{r} - \mathbf{r}')$ is a scalar and Eq. (1) is reduced to $p_{z1}e^{inka} + p_{z1}e^{i(n+1)ka} + p_{z2}e^{i(n+1/2)ka} = 0$, which is exactly the same condition found for electronic graphene [11]. This is why the edge state behavior of the out-of-plane mode is so similar to that of electronic graphene ribbons. The ratio p_{z2}/p_{z1} is simply given by $-2\cos ka$ and is shown by the light gray (green) line in Fig. 3(a). For the in-plane dipole mode, the QSA dyadic dipolar Green function can be written as $\mathbf{G}^{\text{P}}(\mathbf{r} - \mathbf{r}')\mathbf{P}_{\text{in}}(\mathbf{r}') = [3(\mathbf{n} \cdot \mathbf{P}_{\text{in}})\mathbf{n} - \mathbf{P}_{\text{in}}]/|\mathbf{r} - \mathbf{r}'|^3$, where \mathbf{n} is a unit vector along the $\mathbf{r} - \mathbf{r}'$ direction, and \mathbf{T} is a 2×2 matrix that can be found analytically. In Fig. 3(a), the absolute values of the two eigenvalues are

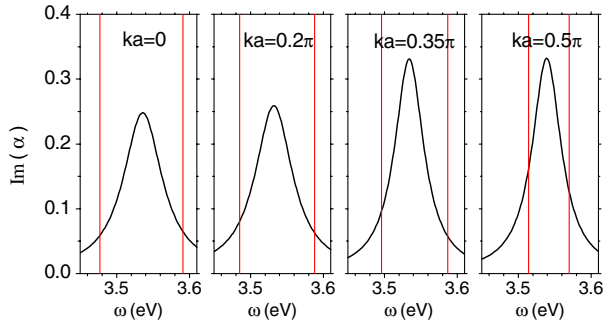


FIG. 4 (color online). Imaginary part of the eigenpolarizability (black curves) for the edge states of the in-plane dipole modes. The corresponding band edges are indicated by gray (red) lines. For these edge states with ω near 3.53 eV, the light line intersects at about $ka = 0.34\pi$.

plotted by a dark gray (red) curve and a black curve. The black curve is always larger than 1, while the dark gray (red) curve is smaller than 1 when $ka < 2\pi/3$, denoted as \mathbf{P}_1 in the figure, which explains why in-plane dipolar edge states are confined by $0 \leq ka < 2\pi/3$. For quadrupoles, there are five independent variables $\{Q_{yy}, Q_{zz}, Q_{xy}, Q_{xz}, Q_{yz}\}$ and the \mathbf{T} matrix is a 5×5 matrix, and the absolute values of the five eigenvalues are plotted in Fig. 3(b). Only two sets of eigenvalues give absolute values less than 1 and thus form edge states. The edge state solution labeled as \mathbf{Q}_1 (blue curve) is smaller than unity in the whole 1D BZ. This corroborates the existence of an edge state band that goes from $ka = 0$ to π in Fig. 2(c) in the $N = 10$ zigzag plasmonic ribbon. Another state denoted by \mathbf{Q}_2 (red curve) has a critical value for the edge state at $ka = 2\pi/3$ similar to the in-plane dipole mode \mathbf{P}_1 .

We note that the absorption and retardation are ignored in the band structure calculations above. In order to see the effects of absorption and radiation, we choose the damping term $\gamma = 0.05$ eV in the Drude model and calculate the eigenpolarizability α [16] for the edge states using a fully dynamical approach. Figure 4 shows $\text{Im}(\alpha)$ (basically a spectral function) of in-plane dipolar edge states for four different values of ka . The $\text{Im}(\alpha)$ is a delta function if there is no loss, but becomes broadened into a Lorentzian if there are absorption and radiation. Since the edge states always exist inside a gap, the corresponding band edges that define the gap are indicated by gray (red) lines in Fig. 4. The edge states should still be well defined as long as the smearing is smaller than the width of the gap. For these edge states with ω near 3.53 eV, the light line intersects at $\omega a/c = 0.34\pi$. For $ka = 0.35\pi$ outside the light cone, the smearing which comes entirely from absorption is smaller than the gap. As k increases, the gap becomes narrower, which is close to the half-width of the edge state at $ka = 0.5\pi$. It is interesting to note that even for $ka = 0$ and 0.2π , which are inside

the light cone, the edge states are still well defined. This is because the gap is bigger than that in large k , and more importantly, the plasmonic nanoparticles are small and the radiation loss (contributes about 0.015 eV to the half-widths) is not significant compared with the absorption loss.

In summary, we have found Dirac spectra in “graphene-like” plasmonic structures for both dipole and quadrupole coupling. Edge states for plasmonic lattices with finite widths are also identified and analyzed numerically and their existence conditions are derived analytically. These results can lead to the study of Dirac point behavior in yet another class of interesting material. The edge states provide new propagation channels of light for a specific range of frequencies. These edge modes and their light transport properties can be characterized by local probes such as the photon scanning tunneling microscope [17].

This work was supported by the Central Allocation Grant from the Hong Kong RGC through HKUST3/06C. Computation resources were supported by the Shun Hing Education and Charity Fund. We thank Dr. Xianyu Ao and Dr. Kin Hung Fung for helpful discussions.

-
- [1] U. Kreibig and M. Vollmer, *Optical Properties of Metal Clusters* (Springer, New York, 1995).
 - [2] S. A. Maier, *Plasmonics: Fundamentals and Applications* (Springer, New York, 2007).
 - [3] S. Nie and S. R. Emory, *Science* **275**, 1102 (1997).
 - [4] K. Kneipp *et al.*, *Phys. Rev. Lett.* **78**, 1667 (1997).
 - [5] P. Anger, P. Bharadwaj, and L. Novotny, *Phys. Rev. Lett.* **96**, 113002 (2006).
 - [6] S. A. Maier *et al.*, *Nature Mater.* **2**, 229 (2003).
 - [7] A. Tao, P. Sinsermsuksakul, and P. D. Yang, *Nature Nanotech.* **2**, 435 (2007).
 - [8] W. Y. Zhang *et al.*, *Phys. Rev. Lett.* **84**, 2853 (2000).
 - [9] K. S. Novoselov *et al.*, *Science* **306**, 666 (2004).
 - [10] Y. W. Son, M. L. Cohen, and S. G. Louie, *Nature (London)* **444**, 347 (2006).
 - [11] K. Nakada *et al.*, *Phys. Rev. B* **54**, 17954 (1996).
 - [12] M. Plihal and A. A. Maradudin, *Phys. Rev. B* **44**, 8565 (1991).
 - [13] F. D. M. Haldane and S. Raghu, *Phys. Rev. Lett.* **100**, 013904 (2008).
 - [14] Z. Wang *et al.*, *Phys. Rev. Lett.* **100**, 013905 (2008).
 - [15] S. Y. Park and D. Stroud, *Phys. Rev. B* **69**, 125418 (2004); W. H. Weber and G. W. Ford, *Phys. Rev. B* **70**, 125429 (2004); D. S. Citrin, *Nano Lett.* **4**, 1561 (2004); A. Alu and N. Engheta, *Phys. Rev. B* **74**, 205436 (2006); A. F. Koenderink and A. Polman, *Phys. Rev. B* **74**, 033402 (2006); V. A. Markel and A. K. Sarychev, *Phys. Rev. B* **75**, 085426 (2007).
 - [16] K. H. Fung and C. T. Chan, *Opt. Lett.* **32**, 973 (2007); Y. R. Zhen, K. H. Fung, and C. T. Chan, *Phys. Rev. B* **78**, 035419 (2008).
 - [17] J. R. Krenn *et al.*, *Phys. Rev. Lett.* **82**, 2590 (1999).